2026 IEEE Intelligent Vehicles Symposium (IV)
June 22-25, 2026. Detroit, MI, USA

Controlling the nonlinear dynamics of trailer sway*

Máté B. Vizi[1], Illés Vörös[1], Bo Yu[2], Tucker Biallas[2], Peter J. Richmond[2], and Gábor Orosz[1,3]

2026 IEEE Intelligent Vehicles Symposium (IV) | 979-8-3315-4793-6/26/$31.00 ©2026 IEEE | DOI: 10.1109/IV66570.2026.11623936

***Abstract*—Trailer sway, observed in experiments, is investigated in this work. A single-track nonlinear model is established which captures the tractor-trailer interaction and accommodates a time-dependent velocity profile. The nonlinear behavior is analyzed using bifurcation analysis and speed ranges of bistable behavior are identified where trailer sway may be induced by applying large enough perturbations. It is demonstrated that via appropriate steering control one may push these dangerous bistable regions to higher speed ranges, but this strategy is sensitive to the time delay in the control loop. It is shown that braking with appropriate deceleration may eliminate trailer sway but the vibration amplitude may increase significantly during braking. We demonstrate that there is an optimal way of combining braking and steering in order to mitigate the sway.**

I. Introduction

Trailer sway refers to the large amplitude oscillation of a tractor-trailer system, which usually happens at highway speed and may lead to serious accidents. This motivates the development of advanced driving assistant systems (ADAS) for trailer sway detection and mitigation. However, the elasticity of the tires and interaction between the tractor and the trailer makes it challenging to construct models that can reproduce the nonlinear behavior, while still being simple enough for control design. In this paper, we make a stride in solving this challenging problem.

The lateral instabilities of human-driven vehicles (including tire elasticity but without trailer) are investigated, for example, in [1]–[4]. Similar phenomenon is observed in teleoperation [5] and in automated vehicles. In all cases, the time delay in the control loop (arising from human drivers or from automation) plays a crucial role in developing the instabilities [6]–[8]. The dynamics becomes even more intricate if we also consider that the vehicle is towing a trailer. The trailer-sway phenomena drew the attention of researchers, and it has been analyzed from various perspectives in the literature [9]–[12]. The roles of tire dynamics have been considered in tractor-trailer systems using various tire models [13]–[15]. In addition, the effects of friction at the hitch point was studied in [16] and the effect of braking was investigated in [17]. The interplay between a lane-keeping controller of the car and an attached trailer was investigated in [9], while the effects of the suspension dynamics were explored in [10].

*This research was supported by the Hyundai America Technical Center, Inc.

[1]Máté Vizi, Illés Vörös, and Gábor Orosz are with the Department of Mechanical Engineering, University of Michigan, Ann Arbor, MI 48109, USA {mvizi, illesvoe, orosz}@umich.edu.

[2]Bo Yu, Tucker Biallas, and Peter Richmond are with the Hyundai America Technical Center, Inc., Superior Township, MI 48198, USA. {boyu, tbiallas, prichmond}@hatci.com.

[3]G. Orosz is also with the Department of Civil and Environmental Engineering, University of Michigan, Ann Arbor, MI 48109, USA.

Most models in the literature fail to capture the intricate behavior that trailer sway can appear and disappear in seemingly unpredictable ways. The analysis is typically restricted to the linear stability of the straight running motion, and the corresponding control design is also often limited to linear techniques, without considering the time delay in the control loop. Moreover, nonlinear analysis is usually only performed using numerical simulations. However, this approach is unable to explain how certain perturbations can lead to sway even when the straight running motion is stable in the linear sense. In order to provide an accurate description of this phenomenon, a sufficiently detailed nonlinear model of the system is required, which is then shall be analyzed using the appropriate tool set.

To respond to these challenges, in this paper, we present a new modeling approach which enables us to capture tractor-trailer interactions while eliminating the need to compute the corresponding constraining forces. This approach also allows us to prescribe a time-dependent speed and delivers first-order nonlinear differential equations ready for analysis and control design. To reveal the stable and unstable motions that constitute the skeleton of the nonlinear dynamics, we perform bifurcation analysis. This enables us to identify bistable regions where trailer sway can be triggered by large enough perturbations. The results of bifurcation analysis are used to design steering and braking controllers at the nonlinear level. When designing feedback laws for the steering control, we also take into account the time delay in the control loop and analyze its effects on the linear and nonlinear dynamics. Braking, on the other hand, is applied in an open loop fashion in order to find the best deceleration rate. The optimal blend of steering and braking is identified in terms of trailer sway elimination.

II. Experimental Results

To motivate the modeling, analysis, and control design presented below, we present our experimental results performed at a closed track, see Fig. 1. Panel (a) illustrates that in certain velocity range the driver can induce trailer sway by applying a rapid perturbation on the steering, even though the straight running motion is stable. Such phenomenon indicates bistable behavior of the system, which can only happen in nonlinear systems, and presents challenges both for modeling and for control design. Panel (b) shows a scenario where the sway develops spontaneously for higher speed, and once the driver tries to eliminate it by reducing the speed, the oscillation amplitude initially increases. This indicates a coupling between the longitudinal and lateral dynamics of tractor trailer systems which makes sway elimination more challenging.

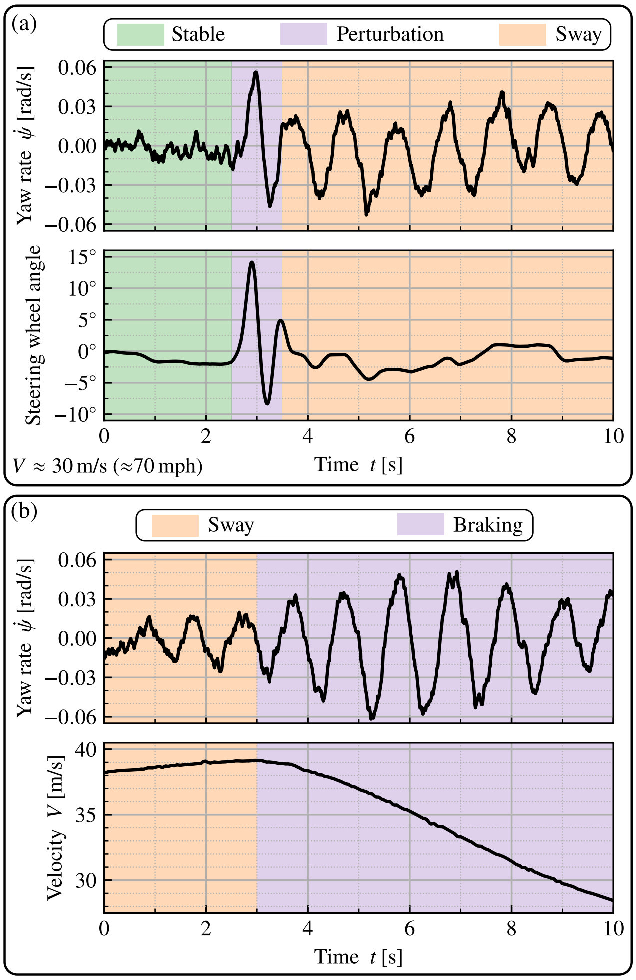

Fig. 1. Trailer sway measurement on a real vehicle: (a) sway triggered by applying a perturbation in the steering angle, (b) effect of braking on spontaneous sway that occurred at higher speed.

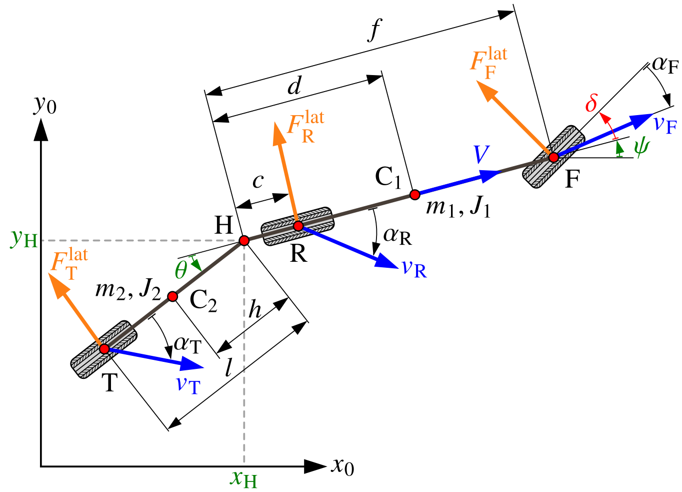

Fig. 2. Single track model of the tractor-trailer system

III. Modeling and Governing Equations

A single-track model encompassing the tractor and the trailer is constructed, meaning that the left and right wheels are replaced by a single wheel that is placed in the middle of the corresponding axles, see Fig. 2. Points F, R, and T represent the centers of the front, rear, and trailer wheels. The hitch point H connects the truck to the trailer with a friction-less revolute joint. The parameters m_1 and J_1 are the mass and mass moment of inertia of the tractor (including the occupants), and point C_1 marks its center of gravity. Similarly, the mass m_2 and the mass moment of inertia J_2 represent the trailer (with load), and point C_2 marks its center of gravity. The steering angle is denoted by δ, while the lengths c, d, f, h, and l are geometric parameters. The values of the physical parameters can be found in Table I.

The spatial configuration of the tractor-trailer system can be unambiguously characterized by the position $(x_{\mathrm{H}}, y_{\mathrm{H}})$ of the hitch point H, the yaw angle ψ of the tractor, and the relative yaw angle (called the hitch angle) θ of the trailer. That is, the generalized coordinates are chosen to be

$$x_{\mathrm{H}}\,, \quad y_{\mathrm{H}}\,, \quad \psi\,, \quad \theta. \tag{1}$$

TABLE I
Physical Parameters Considered in This Work

$m_1 = 2400\,\mathrm{kg}$	$J_1 = 7647\,\mathrm{kgm}^2$	$d = 3.25\,\mathrm{m}$
$m_2 = 985\,\mathrm{kg}$	$J_2 = 1416\,\mathrm{kgm}^2$	$h = 2.9\,\mathrm{m}$
$f = 5.15\,\mathrm{m}$	$c = 1.35\,\mathrm{m}$	$l = 2.8\,\mathrm{m}$
$C_{\mathrm{F}} = 137\,\mathrm{kN}$	$C_{\mathrm{R}} = 256\,\mathrm{kN}$	$C_{\mathrm{T}} = 50\,\mathrm{kN}$

It is assumed that the tires only deform in the lateral direction, and the brush tire model is assumed to characterize the tire behavior. The lateral force F^{lat} is given as the function (see (14) in the Appendix) of the slip angle α which gives the misalignment between the wheel plane and the velocity vector of the wheel center, see Fig. 2. The slip angles can be obtained from the vehicle kinematics:

$$\begin{aligned}
\alpha_{\mathrm{F}} &= \delta + \psi - \operatorname{atan} \frac{\dot{y}_{\mathrm{H}} + \dot{\psi} f \cos\psi}{\dot{x}_{\mathrm{H}} - \dot{\psi} f \sin\psi}, \\
\alpha_{\mathrm{R}} &= \psi - \operatorname{atan} \frac{\dot{y}_{\mathrm{H}} + \dot{\psi} c \cos\psi}{\dot{x}_{\mathrm{H}} - \dot{\psi} c \sin\psi}, \\
\alpha_{\mathrm{T}} &= \psi + \theta - \operatorname{atan} \frac{\dot{y}_{\mathrm{H}} - \big(\dot{\psi} + \dot{\theta}\big)\, l \cos(\psi + \theta)}{\dot{x}_{\mathrm{H}} + \big(\dot{\psi} + \dot{\theta}\big)\, l \sin(\psi + \theta)},
\end{aligned} \tag{2}$$

where the subscripts F, R, and T refer to the front, rear, and trailer tires, respectively. The corresponding lateral tire forces are $F_{\mathrm{F}}^{\mathrm{lat}}$, $F_{\mathrm{R}}^{\mathrm{lat}}$, and $F_{\mathrm{T}}^{\mathrm{lat}}$.

The time-dependent longitudinal velocity of the tractor is prescribed as $V(t)$, which leads to the kinematic constraint

$$\dot{x}_{\mathrm{H}} \cos\psi + \dot{y}_{\mathrm{H}} \sin\psi - V = 0\,, \tag{3}$$

yielding a nonholonomic mechanical system. We utilize the Appellian approach [18], [19] that yields a set of first-order ordinary differential equations, ready for bifurcation analysis and control design. We introduce the pseudovelocities

$$\begin{aligned}
\sigma_1 &:= -\dot{x}_{\mathrm{H}} \sin\psi + \dot{y}_{\mathrm{H}} \cos\psi\,, \\
\sigma_2 &:= \frac{m_1 d}{J_1}\big(-\dot{x}_{\mathrm{H}} \sin\psi + \dot{y}_{\mathrm{H}} \cos\psi\big) + \dot{\psi}\,, \\
\sigma_3 &:= \frac{m_2 h}{J_2}\big(\dot{x}_{\mathrm{H}} \sin\psi - \dot{y}_{\mathrm{H}} \cos\psi\big) \cos\theta + \dot{\psi} + \dot{\theta}\,,
\end{aligned} \tag{4}$$

where σ_1 is the lateral velocity of the hitch point H and we defined the constants $I_1 := J_1 + m_1 d^2$ and $I_2 := J_2 + m_2 h^2$. Combining (4) with the kinematic constraint (3) gives the kinematic part of the equations of motion:

$$
\begin{aligned}
\dot{x}_{\mathrm{H}} &= V \cos\psi - \sigma_1 \sin\psi\,,\\
\dot{y}_{\mathrm{H}} &= V \sin\psi + \sigma_1 \cos\psi\,,\\
\dot{\psi} &= -\frac{1}{I_1}\big(\sigma_1 m_1 d - \sigma_2 I_1\big)\,,\\
\dot{\theta} &= \frac{1}{I_1 I_2}\Big(\sigma_1\big(m_2 h I_1 \cos\theta + m_1 d I_2\big) - (\sigma_2 - \sigma_3) I_1 I_2\Big)\,.
\end{aligned} \tag{5}
$$

Due to the lengthy calculation, the steps of the derivation of the dynamical equations are omitted here. These become

$$
\begin{aligned}
\dot{\sigma}_1 &= \frac{1}{D(\theta)}\Big(\big(\sigma_1\sigma_2 - 2\sigma_1\sigma_3 - \dot{V}\big) p_1 \sin\theta\cos\theta\\
&\quad - \sigma_1^2\big(p_2 + p_3\cos\theta\big)\sin\theta\cos\theta - \sigma_3^2 p_4 \sin\theta\\
&\quad + V\big(\sigma_1 p_5 - \sigma_2 I_1\big)\big(p_6 + p_7\sin^2\theta\big) + F_{\mathrm{R}}^{\mathrm{lat}} p_8\\
&\quad + F_{\mathrm{T}}^{\mathrm{lat}} p_9 \cos\theta + F_{\mathrm{F}}^{\mathrm{lat}} p_{10}\cos\delta\Big)\,,\\
\dot{\sigma}_2 &= \frac{1}{I_1^2}\Big(V\sigma_1 p_5^2 - V\sigma_2 p_{11} + F_{\mathrm{R}}^{\mathrm{lat}} I_1 c + F_{\mathrm{F}}^{\mathrm{lat}} I_1 f\cos\delta\Big)\,,\\
\dot{\sigma}_3 &= \frac{1}{I_1 I_2^3}\Big(\sigma_1^2 p_{12}\sin\theta\cos\theta + V\big(\sigma_2 p_{13} - \sigma_1 p_{14}\big)\cos\theta\\
&\quad + \big(\sigma_1\sigma_3 - \dot{V}\big) p_{13}\sin\theta - F_{\mathrm{T}}^{\mathrm{lat}} p_{15}\Big)\,,
\end{aligned} \tag{6}
$$

where

$$
\begin{aligned}
&p_1 = m_2^2 I_1^2 I_2^2 h^2, \quad p_2 = m_1 m_2^2 I_1 I_2^2 d h^2, \quad p_3 = m_2^3 I_1^2 I_2 h^3,\\
&p_4 = m_2 I_1^2 I_2^3 h, \quad p_5 = m_1 d, \quad p_6 = \big(m_1 J_1 I_2 + m_2 I_1 J_2\big) I_2^2,\\
&p_7 = m_2^2 I_1 I_2^2 h^2, \quad p_8 = \big(J_1 + m_1 d(d-c)\big) I_1 I_2^3,\\
&p_9 = \big(J_2 + m_2 h(h-l)\big) I_1^2 I_2^2, \quad p_{10} = \big(J_1 + m_1 d(d-f)\big) I_1 I_2^3,\\
&p_{11} = m_1 I_1 d, \quad p_{12} = m_2^2 I_1 I_2 h^2, \quad p_{13} = m_2 I_1 I_2^2 h,\\
&p_{14} = m_1 m_2 I_2^2 h d, \quad p_{15} = I_1 I_2^2 l,\\
&D(\theta) = I_2\Big(m_1 J_1^2 I_2^2 + m_1^2 J_1 I_2^2 d^2 + m_2^2 J_2 I_1^2 h^2\cos^2\theta\\
&\qquad + m_2 I_1^2\big(J_2^2 + (2 m_2 J_2 h^2 + m_2^2 h^4)\sin^2\theta\big)\Big)\,.
\end{aligned} \tag{7}
$$

Then (5), (6), (7) constitute the equation of motion such that the dependence of the tire forces $F_{\mathrm{F}}^{\mathrm{lat}}, F_{\mathrm{R}}^{\mathrm{lat}}, F_{\mathrm{T}}^{\mathrm{lat}}$ on the slip angles $\alpha_{\mathrm{F}}, \alpha_{\mathrm{R}}, \alpha_{\mathrm{T}}$ (2) is given in the Appendix by (14), (15). Observe that there are four kinematic equations but only three dynamical equations. That is, having a kinematic constraint reduces the number of first-order differential equations by one, resulting in effectively a 3.5 degree-of-freedom system [18]. The compact form of the equation of motion enables us to perform bifurcation analysis and control design at the linear and nonlinear levels.

IV. Dynamics and Control of Trailer Sway

In this section, we perform bifurcation analysis to identify stable and unstable motions that constitute the skeleton of the dynamics. We start with the open-loop system without steering control, followed by control design and the subsequent bifurcation analysis of the closed-loop system.

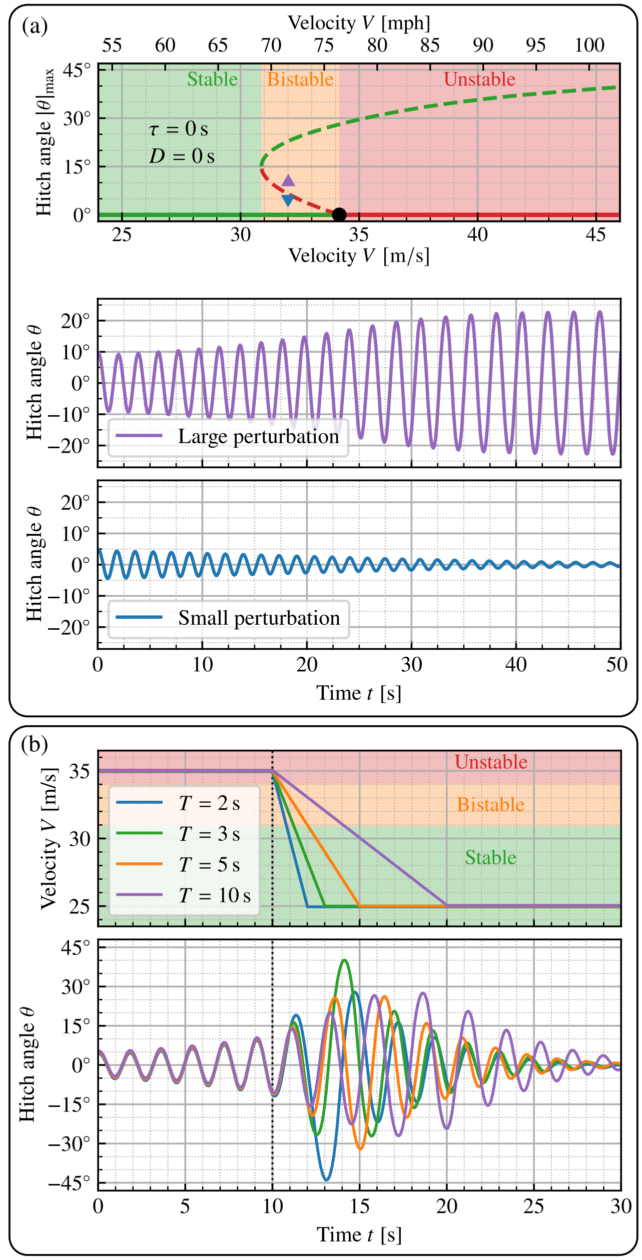

Fig. 3. Open loop behavior: (a) bifurcation diagram and numerical simulations demonstrating the bistability by using small and large perturbations in the hitch angle θ, (b) effect of braking with various deceleration rates.

A. Open-loop behavior

The nonlinear system (5), (6), (7) with definitions (2), (14), (15) has seven states: $\sigma_1, \sigma_2, \sigma_3, \theta, \psi, x_{\mathrm{H}}, y_{\mathrm{H}}$, and two inputs: the steering angle δ and the longitudinal velocity V. We start our analysis with the special case $\delta \equiv 0$ and $V \equiv$ const, which we refer to as the open-loop system. We utilize the numerical continuation software DDE-Biftool [20] to find equilibria and periodic orbits, evaluate their stability, and continue them as parameters are varied.

The top panel in Fig. 3(a) shows the results when using velocity V as a bifurcation parameter and plotting the amplitude of the hitch angle θ. The horizontal axis corresponds to the straight running equilibrium where all states are zero except $x = Vt$. Below the critical velocity $V_{\mathrm{crit}} \approx 34.1$ m/s, this state is stable (as indicated by solid green line) and it is unstable above (as shown by solid red line). The stability change occurs via a subcritical Hopf bifurcation (marked by a black dot). As a result, a branch of unstable limit cycle arises (dashed red curve) above the stable equilibrium. This branch eventually folds back and the limit cycle becomes stable (dashed green curve). The corresponding stable oscillations are referred to as trailer sway.

Based on the bifurcation diagram, we can differentiate three different velocity regions: stable, unstable, and bistable, which are indicated by green, red, and orange shadings. In the stable region, the straight running equilibrium is globally stable, that is, no sway arises even if one tries to trigger one. In the unstable region, the equilibrium is unstable and the system converges to the stable limit cycle, that is, sway arises spontaneously. In the bistable region, both the straight running motion and the sway motion are stable, and depending on the initial condition, the system converges to one or the other. For small perturbations, the system returns to the equilibrium, but sway can be triggered with large enough perturbations. The unstable limit cycle provides the threshold on how large perturbation is needed. The bottom panels of Fig. 3(a) illustrate this phenomenon in the hitch angle θ, cf. the measurements in Fig. 1(a). We note that the measured sway amplitudes agree with our theoretical predictions, while the vibration frequencies are somewhat off.

In the unstable region, sway arises spontaneously. As a response, one may try to reduce the speed to travel through the bistable region to the stable one. The effect of braking (in an open-loop fashion) is illustrated in Fig. 3(b). As shown in the top panel, four velocity profiles are considered that differ in the deceleration rate: the velocity is decreased by 10 m/s in $T \in \{2, 3, 5, 10\}$ seconds. The bottom panel shows the time evolution of the hitch angle θ. In case of strong braking ($T = 2$ s, 3 s) the hitch angle increases rapidly even in the stable velocity regime, therefore it is not advised. In case of slight braking ($T = 10$ s), the sway lasts longer as the system spends more time in the problematic velocity regime. Moderate braking ($T = 5$ s) seems to be a good compromise between eliminating the sway quickly without increasing the hitch angle too much, cf. the measurements in Fig. 1(b).

B. Closed-loop control

As shown above, the open-loop braking strategy has its limitations in eliminating trailer sway, and it also leads to lower travel speed which is not always desirable. Here, we design a feedback law for the steering angle and analyze its impact on the dynamics. Then we combine this with braking to find the most effective way of sway mitigation.

In a tractor-trailer system, the yaw rate of the tractor is typically the only state accessible through direct measurement. Accordingly, we consider the feedback law

$$\delta(t) := -D\dot{\psi}(t - \tau), \tag{8}$$

where D is the control gain and τ is the time delay due to sensing, computation, and actuation. In production vehicles, this delay is in the range of 0.2–0.4 s [21], [22]. Other, more sophisticated control algorithms involving more system states either require more sensors, thereby increasing the cost; or they require the implementation of state observers which is challenging due to the highly nonlinear nature of the system and would also increase the delay in the control loop.

Below we analyze the dynamics of the closed loop system while varying the control gain D, the time delay τ, and the longitudinal velocity V, where the latter is considered constant in time. First, we focus on the linear stability of the straight running equilibrium and then investigate the limit cycle oscillations using bifurcation analysis.

We linearize the closed loop system (5), (6), (7), (8) about the equilibrium (with constant speed V). This results in

$$\begin{aligned} \dot{\mathbf{x}}(t) &= \mathbf{A}\mathbf{x}(t) + \mathbf{B}u(t), \\ y(t) &= \mathbf{C}\mathbf{x}(t), \end{aligned} \tag{9}$$

where

$$\begin{aligned} \mathbf{x} &= \left[\begin{array}{cccc|ccc} \sigma_1 & \sigma_2 & \sigma_3 & \theta & \psi & \tilde{x}_{\mathrm{H}} & y_{\mathrm{H}} \end{array} \right]^{\mathsf{T}}, \\ u &= \delta, \qquad y = \dot{\psi}, \end{aligned} \tag{10}$$

and $\tilde{x}_{\mathrm{H}} = x_{\mathrm{H}} - Vt$. The corresponding system, input, and output matrices are in the form

$$\begin{aligned} \mathbf{A} &= \left[\begin{array}{cccc|ccc} A_{11} & A_{12} & A_{13} & A_{14} & 0 & 0 & 0 \\ A_{21} & A_{22} & 0 & 0 & 0 & 0 & 0 \\ A_{31} & A_{32} & A_{33} & A_{34} & 0 & 0 & 0 \\ A_{41} & A_{42} & A_{43} & 0 & 0 & 0 & 0 \\ \hline A_{51} & A_{52} & 0 & 0 & 0 & 0 & 0 \\ 0 & 0 & 0 & 0 & 0 & 0 & 0 \\ A_{71} & 0 & 0 & 0 & A_{75} & 0 & 0 \end{array} \right], \\ \mathbf{B} &= \left[\begin{array}{cccc|ccc} B_1 & B_2 & 0 & 0 & 0 & 0 & 0 \end{array} \right]^{\mathsf{T}}, \\ \mathbf{C} &= \left[\begin{array}{cccc|ccc} -\frac{m_1 d}{I_1} & 1 & 0 & 0 & 0 & 0 & 0 \end{array} \right], \end{aligned} \tag{11}$$

where the elements of $\mathbf{A}$ and $\mathbf{B}$ can be obtained analytically, but since these are rather complicated and lengthy, they are not spelled out here. We emphasize, however, that the system matrix $\mathbf{A}$ depends strongly on the longitudinal velocity V. The matrix $\mathbf{C}$ is constructed based on (4).

Using the feedback law (8) in (9), we obtain

$$\dot{\mathbf{x}}(t) = \mathbf{A}\mathbf{x}(t) - \mathbf{B}D\mathbf{C}\mathbf{x}(t - \tau), \tag{12}$$

which is a delay differential equation describing the closed loop dynamics. The stability of the delay-free system ($\tau = 0$) is decided based on the eigenvalues of the matrix $\bar{\mathbf{A}} - \bar{\mathbf{B}}D\bar{\mathbf{C}}$, where overbar denotes the first 4 elements or 4×4 part of $\mathbf{A}$, $\mathbf{B}$, $\mathbf{C}$ (as the development of trailer sway does not depend on the position and orientation of the vehicle). When all four eigenvalues are located in the left-half complex plane, the equilibrium is linearly stable. The stability with time delay ($\tau > 0$) can be determined using the characteristic equation

$$\det\left(\lambda\mathbf{I} - \bar{\mathbf{A}} + \bar{\mathbf{B}}D\bar{\mathbf{C}}\mathrm{e}^{-\lambda\tau}\right) = 0\,. \tag{13}$$

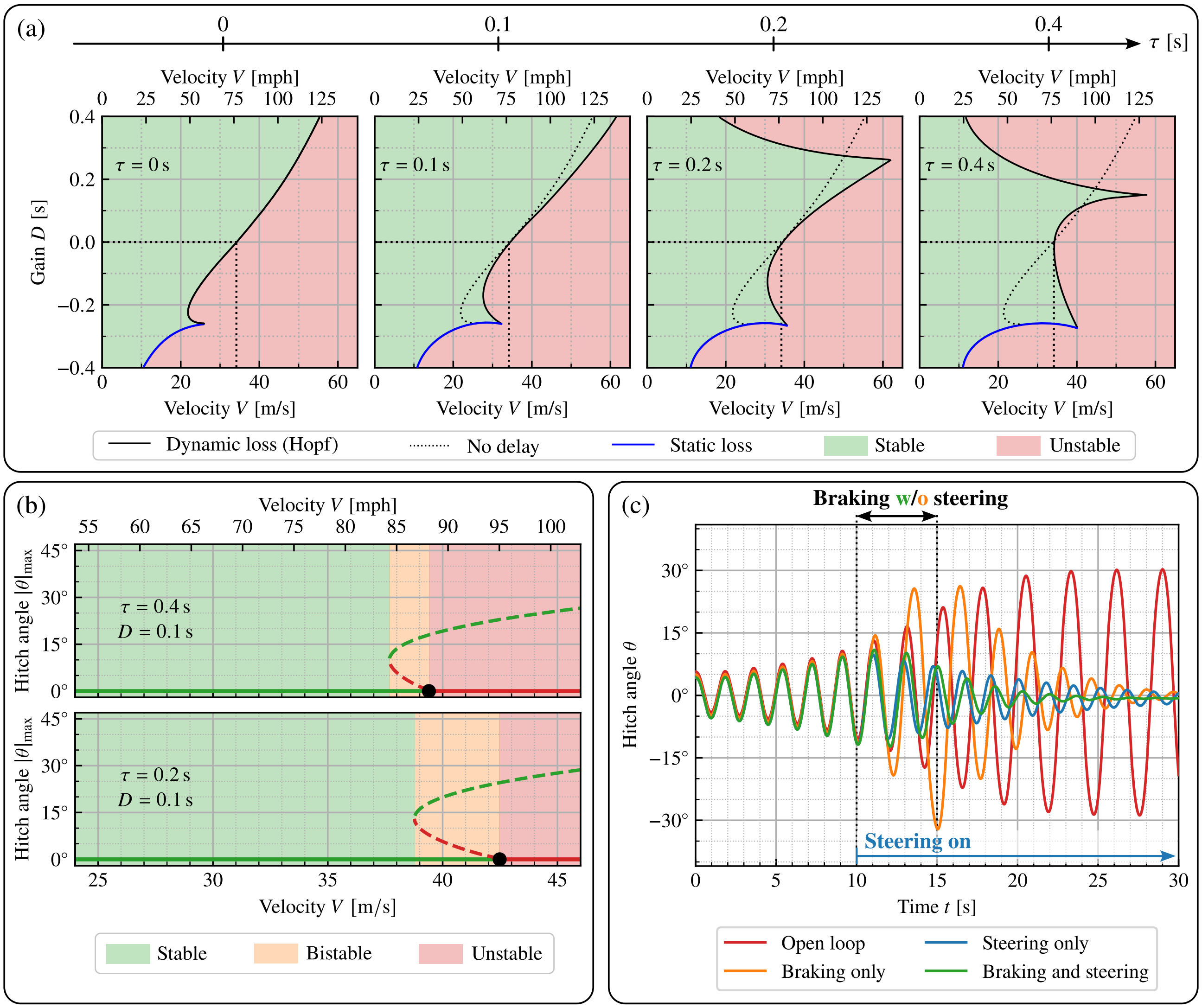

Fig. 4. Closed loop behavior: (a) stability of the equilibrium under yaw rate feedback for different values of the delay, (b) bifurcation diagrams comparing different time delays and feedback gains, (c) suppressing the trailer sway with braking, steering, and the combination of those.

In this case, if all of the infinitely many characteristic roots λ are on the left-half complex plane, the equilibrium is stable. Here, we utilize semi-discretization [23] to compute finitely many leading characteristic roots to determine stability.

Figure 4(a) shows stability charts in the (V, D)-plane for different values of τ. The green area corresponds to linearly stable equilibrium, while red shading indicates its instability. The blue curve shows the static stability boundary where a real characteristic root becomes positive and the equilibrium becomes unstable. This curve does not depend on the delay. The black curves are the dynamic stability boundaries where a complex conjugate pair of characteristic roots crosses the imaginary axis, corresponding to the Hopf bifurcation discussed above. The dynamic stability boundary of $\tau = 0$ is reproduced as a dotted black curve in the $\tau > 0$ stability charts for the sake of comparison. Observe that, somewhat surprisingly, having a small delay ($\tau = 0.1$ s) increases the stable region in the physically relevant case of $D > 0$. However, for large delay values the system becomes more unstable and the corresponding critical velocity may be significantly smaller compared even to the open-loop case. This illustrates the intricacy brought by the time delay into this control system, demanding further efforts to ensure that sway can be avoided for higher delay values. Furthermore, quasiperiodic motions are expected in the vicinity of the sharp corners of the stability boundary. This additional intricate behavior of the tractor-trailer system also demands further analysis.

Now we apply the controller (8) to the full nonlinear system (5), (6), (7) and perform bifurcation analysis. The numerical continuation software DDE-Biftool [20] is used again, to find and continue the branches of stable and unstable limit cycle oscillations. Figure 4(b) shows that the controller increases the critical speed of linear stability loss while it also pushes the bistable region to higher velocities.

Figure 4(c) shows numerical simulations that present the advantages of combining braking with the proposed steering controller. The initial velocity is $V(0) = 35\,\mathrm{m/s}$, which is in the linearly unstable regime. Without any action (no braking or steering), large amplitude trailer sway develops, see the red curve. When the proposed steering controller (with $\tau = 0.2\,\mathrm{s}$, $D = 0.1\,\mathrm{s}$) is turned on at $t = 10\,\mathrm{s}$, the sway can be eliminated even at large speeds, as illustrated by the blue curve, since the stability is changed by the controller. However, this mitigation technique requires the controller to be turned on continuously, otherwise the sway would start to develop again. Considering moderate braking ($T = 5\,\mathrm{s}$, orange velocity profile in Fig. 3(b)) without steering, the trailer sway is also eliminated, but the sway amplitude is further increased at the beginning of braking; see the orange curve. The best result is achieved by combining braking and steering as the fastest decrease of the sway amplitude can be observed in this case, as shown by the green curve. Additionally, this approach allows the controller to be turned off once the system has returned to the stable velocity regime.

V. Conclusion

A nonlinear dynamical model is introduced for tractor-trailer systems that incorporates the tire elasticity and a time varying longitudinal velocity. The strength of this model is that it qualitatively reproduces the bistable phenomena of trailer sway: depending on the initial conditions, trailer sway may or may not occur. The model can also predict the initial increase of the sway amplitude in case of braking. This allows control design for optimal braking and steering at the nonlinear level.

The nonlinear dynamics of trailer sway was investigated without and with yaw rate feedback while taking into account the time delays in the control loop. Linear stability investigations revealed that the effects of time delays may be counterintuitive, since having small delays may in fact improve stability while larger delays may destroy it. Moreover, bifurcation investigations were used to find stable and unstable limit cycle oscillations which lead to bistable behavior. It was shown that the proposed controller mitigates such behavior, at least for small delays. The results presented in this paper shed light on the intricate nonlinear nature of trailer sway.

Appendix: Brush Tire Model

The lateral tire force of the brush tire model [18] is expressed as

$$F^{\mathrm{lat}} = \begin{cases} \phi_1 \tan\alpha + \phi_2 \tan^2\alpha \,\mathrm{sgn}\,\alpha + \phi_3 \tan^3\alpha & \text{if } |\alpha| \le \alpha_{\mathrm{cr}}\,, \\ F_z \mu \,\mathrm{sgn}\,\alpha & \text{if } |\alpha| > \alpha_{\mathrm{cr}}\,, \end{cases} \tag{14}$$

with

$$\begin{aligned} \phi_1 &= C\,, & \alpha_{\mathrm{cr}} &= \mathrm{atan}\left(\tfrac{3F_z\mu_0}{C}\right), \\ \phi_2 &= \tfrac{C^2}{3F_z\mu_0}\left(\tfrac{\mu}{\mu_0} - 2\right), & \phi_3 &= \tfrac{C^3}{9F_z^2\mu_0^2}\left(1 - \tfrac{2\mu}{3\mu_0}\right), \end{aligned} \tag{15}$$

where F_z is the vertical load of the tire, C is the cornering stiffness, while $\mu_0 = 0.9$ and $\mu = 0.6$ are the static and dynamic dry friction coefficients.

Acknowledgment

We thank Dénes Takács, Heeseong Kim, and Xunbi Ji for the fruitful discussions about trailer sway.

References

[1] F. Della Rossa and G. Mastinu, "Analysis of the lateral dynamics of a vehicle and driver model running straight ahead," *Nonlinear Dynamics*, vol. 92, no. 1, pp. 97–106, 2018.

[2] ——, "Straight ahead running of a nonlinear car and driver model–new nonlinear behaviours highlighted," *Vehicle System Dynamics*, vol. 56, no. 5, pp. 753–768, 2018.

[3] A. Steindl, J. Edelmann, and M. Plöchl, "Limit cycles at oversteer vehicle," *Nonlinear Dynamics*, vol. 99, pp. 313–321, 2020.

[4] G. Mastinu, D. Biggio, F. Della Rossa, and M. Fainello, "Straight running stability of automobiles: experiments with a driving simulator," *Nonlinear Dynamics*, vol. 99, no. 4, pp. 2801–2818, 2020.

[5] X. A. Ji, S. S. Avedisov, M. I. Khan, I. Vörös, O. Altintas, and G. Orosz, "On the effects of latency in teleoperated driving: stability and performance analysis," *Vehicle System Dynamics*, 2025.

[6] S. Beregi, S. S. Avedisov, C. R. He, D. Takács, and G. Orosz, "Connectivity-based delay-tolerant control of automated vehicles: theory and experiments," *IEEE Transactions on Intelligent Vehicles*, vol. 8, no. 1, pp. 275–289, 2023.

[7] H. Lu, G. Stépán, J. Lu, and D. Takács, "Dynamics of vehicle stability control subjected to feedback delay," *European Journal of Mechanics-A/Solids*, vol. 96, p. 104678, 2022.

[8] I. Vörös, D. Takács, and G. Orosz, "Safe lane-keeping with feedback delay: bifurcation analysis and experiments," *IEEE Control Systems Letters*, vol. 7, pp. 1147–1152, 2023.

[9] I. Vörös and D. Takács, "The effects of trailer towing on the dynamics of a lane-keeping controller," in *Dynamic Systems and Control Conference*, vol. 1. ASME, 2020, p. V001T02A004.

[10] H. Z. Horváth and D. Takács, "Stability and local bifurcation analyses of two-wheeled trailers considering the nonlinear coupling between lateral and vertical motions," *Nonlinear Dynamics*, vol. 107, no. 3, pp. 2115–2132, 2022.

[11] W. Cho, Y. Yoon, and S.-H. You, "A study on sway stability control methods for tractor-trailer system using rear wheel steering," *IEEE Access*, vol. 12, pp. 66 952–66 963, 2024.

[12] Q. Liu, C. Zhang, T. J. Gordon, and J. Wang, "Dynamics and control of articulated passenger vehicles on roads," *Vehicle System Dynam.*, 2025.

[13] L. Segel and R. D. Ervin, "The influence of tire factors on the stability of trucks and tractor trailers," *Vehicle System Dynamics*, vol. 10, no. 1, pp. 39–59, 1981.

[14] H. Troger and K. Zeman, "A nonlinear analysis of the generic types of loss of stability of the steady state motion of a tractor-semitrailer," *Vehicle System Dynamics*, vol. 13, no. 4, pp. 161–172, 1984.

[15] S. Beregi, D. Takács, and G. Stépán, "Tyre induced vibrations of the car–trailer system," *Journal of Sound and Vibration*, vol. 362, pp. 214–227, 2016.

[16] R. S. Sharp and M. A. Alonso Fernández, "Car-caravan snaking—part 1: The influence of pintle pin friction," *Proceedings of the Institution of Mechanical Engineers, Part C*, vol. 216, no. 7, pp. 707–722, 2002.

[17] R. S. Sharp and M. A. A. Fernández, "Car—caravan snaking—part 2: Active caravan braking," *Proceedings of the Institution of Mechanical Engineers, Part C*, vol. 216, no. 7, pp. 723–736, 2002.

[18] G. Orosz, I. Vörös, and D. Takács, "On the handling dynamics of automated vehicles: an Appellian view," in *Vehicle Dynamics, Control and Design*, B. Lenzo and F. Naets, Eds. Springer, 2025, pp. 221–280.

[19] M. B. Vizi, G. Orosz, D. Takács, and G. Stépán, "Steering control of an autonomous unicycle," *IEEE Transactions on Control Systems Technology*, vol. 33, no. 6, pp. 2393–2409, 2025.

[20] J. Sieber, K. Engelborghs, T. Luzyanina, G. Samaey, and D. Roose, "DDE-Biftool Manual – Bifurcation analysis of delay differential equations," *arXiv preprint*, 2016, `arXiv:1406.7144`.

[21] S. Xu, H. Peng, and Y. Tang, "Preview path tracking control with delay compensation for autonomous vehicles," *IEEE Transactions on Intelligent Transportation Systems*, vol. 22, no. 5, pp. 2979–2989, 2021.

[22] Comma.ai, "Openpilot 0.10 release notes: Live lateral delay estimation enabled," 2025, URL: `blog.comma.ai/010release/`.

[23] T. Insperger and G. Stépán, *Semi-discretization for Time-delay Systems*. Springer, 2011.